

The effect of MWA protocols upon morphology and IVIM parameters of hepatic ablation zones—a preliminary in vivo animal study with an MRI-compatible microwave ablation device

Weitao Ye* 
 Wanqun Yang* 
 Chengwei Guo 
 Chenyu Dong 
 Feng Shi 
 Changhong Liang 

PURPOSE

We aimed to explore the effect of microwave ablation (MWA) protocols upon morphology and instant changes in intravoxel incoherent motion (IVIM) diffusion-weighted imaging (DWI) parameters on MWA zones in porcine livers.

METHODS

According to the empirical protocol for MWA in tumors less than 3 cm in our hospital, the power and application duration were assigned as five groups: A, 60 W × 5 min ($n = 6$); B, 80 W × 3 min ($n = 7$); C, 80 W × 5 min ($n = 10$); D, 100 W × 3 min ($n = 10$); E, 100 W × 5 min ($n = 9$). Spearman correlation between MWA protocols, morphological metrics, and instant post-ablation IVIM parameters was performed.

RESULTS

There was fair positive correlation between energy delivery and short axis ($R_{\text{Spearman}} = 0.426$, $P = .005$) of the white zone. There was moderate-to-good positive correlation between wattage and short axis ($R_{\text{Spearman}} = 0.584$, $P < .001$) of the white zone. For post-ablation IVIM parameters in the white zone, only wattage had moderate-to-good positive correlation with D value ($R_{\text{Spearman}} = 0.574$, $P < .001$) or ADC value ($R_{\text{Spearman}} = 0.550$, $P < .001$). No correlation between energy delivery, wattage, duration, and f value was observed ($R_{\text{Spearman}} = 0.185$, $P = .24$; $R_{\text{Spearman}} = -0.001$, $P = .99$; $R_{\text{Spearman}} = 0.203$, $P = .20$, respectively).

CONCLUSION

The increase in the short axis of the white zone is more likely to be affected by wattage than energy delivery. The instant post-ablation IVIM is feasible in monitoring the MWA zones since the f value in the white zones is not sensitive to changes in MWA protocols, which is promising in evaluating the instant effect of MWA.

From the Department of Radiology (W.Y., W. Yang, C.L. ✉ Liangchanghong@gdph.org.cn), Guangdong Provincial People's Hospital, Guangdong Academy of Medical Sciences, Guangdong, People's Republic of China; Department of Radiology (C.G.), 82 Group Hospital of PLA, Hebei, Province, People's Republic of China; Department of Radiology (C.D.), the Third Affiliated Hospital of Sun Yat-Sen University, Guangdong, People's Republic of China; Department of Interventional Radiology (F.S.), Guangdong Provincial People's Hospital, Guangdong Academy of Medical Sciences, Guangdong, People's Republic of China.

*Weitao Ye and Wanqun Yang contributed equally to this work.

Received 7 May 2020; revision requested 17 June 2021; last revision received 6 January 2021; accepted 21 January 2021.

DOI: 10.5152/dir.2022.20292

Imaging-guided microwave ablation (MWA) is an effective and widely used therapeutic option for locoregional solid hepatic tumors.^{1,2} MWA eradicates tumor cells with heat by continuously oscillating the dipole water molecules within the electromagnetic field generated around the antenna.³ It excels in minimal invasiveness when compared with conventional resectional therapy, avoids the influence of electrical impedance which rises dramatically with temperature during radiofrequency ablation, and is less susceptible to the presence of adjacent vessels.⁴⁻⁶

However, excessive heat along the antenna may result in a greater long axis of the MWA zone, causing unnecessary injury in adjacent structures and even skin burns with unbearable pain.⁷ Meanwhile, local tumor recurrence may occur due to unsuccessful eradication of the tumor, especially when the short axis of the white zone (coagulation zone) is smaller than the tumor. Given the fact that most hepatocellular carcinoma lesions and metastatic tumors are round, the clinical demand for an ideal white zone should be as spherical as possible (which is affected by the long and short axes of the white zone at the same time), and large enough with a safe margin of at least 5-10 mm,⁸ while the injury of normal surrounding tissue should be minimal. Therefore, it is of great significance to determine the morphology of the white zone before operation, such as the long and short axes, the area, the sphericity, and even the surrounding hyperemic zone.

You may cite this article as: Ye W, Yang W, Guo C, Dong C, Shi F, Liang C. The effect of MWA protocols upon morphology and IVIM parameters of hepatic ablation zones—a preliminary in vivo animal study with an MRI-compatible microwave ablation device. *Diagn Interv Radiol.* 2022;28(2):115-123.

Previous studies have investigated the effect of power-application duration settings upon the morphological metrics of MWA zones. However, in many of these studies, either one of the parameters (for instance, the wattage or the application duration) was fixed,⁹⁻¹² or they were performed with *ex vivo* liver models.^{13,14} It remains to be specified whether the total energy delivery, the power, or the application duration plays a more important role in the morphology of MWA zones *in vivo*.

On the other hand, the therapeutic effect of MWA can rarely be evaluated by histopathological study of the resected specimen because of its minimal invasiveness. Intravoxel incoherent motion (IVIM)-diffusion-weighted imaging (DWI) is a noninvasive technique which is able to separate the microscopic random motion of water molecules within the tissue (measured by apparent diffusion coefficient, ADC) into pure Brownian motion (measured by true diffusion coefficient, D) and microcirculation within the pseudo-randomly distributed capillary network (measured by perfusion fraction, *f* and pseudo-diffusion coefficient, *D**).¹⁵ Previous studies have demonstrated the feasibility of IVIM or DWI in characterization of the tissue components (coagulative necrosis, inflammatory reaction region, and viable residual tumor) after ablation.¹⁶⁻¹⁹ Nevertheless, in most of these studies, DWI was not performed instantly after ablation, and the interval ranged from at least 60 min to 6 months.^{16-18,20} Hoffmann et al.¹⁹ compared the instant post-ablation mean ADC between hepatic parenchyma,

untreated tumor, and hyperintense rim of hepatic malignancies, but did not evaluate the changes of diffusion parameters in the central necrotic areas. Given the correlation between residual temperature in the MWA zones and diffusion parameters,²¹⁻²³ the potential bias of instant post-ablation IVIM parameters in different MWA protocols remains to be investigated.

Therefore, the purpose of this study was (1) to determine the effect of power-application duration settings upon MWA lesion morphology *in vivo*; (2) to investigate the potential bias of instant post-ablation IVIM parameters in different MWA protocols. An MRI-compatible MWA device was used in porcine livers, with several groups of data containing either the same energy delivery, power (wattage), or application duration.

Methods

Animals

The local research ethics committee approved our animal research (No. GDREC2019379A, 2019), and all the authors complied with NIH guidelines for use of laboratory animals. Nine male Wuzhishan miniature pigs (weight range, 33-43 kg) were included in this study.

After anesthesia with pentobarbital sodium (30 mg/kg, Merck KGaA) and fentanyl citrate (0.05 mg/kg, Fufen, Yichang Humanwell Pharmaceutical) administered through the ear vein, the epigastric area was covered with a home-made orientation grid. The pigs were transferred to a 1.5 T Magnetom Espree MRI scanner (Siemens Healthcare) and placed head-first in a lateral decubitus position. A six-element phased-array coil with a sensor for respiratory gating was used.

MWA protocols

All the procedures were performed with an MRI-compatible device (Surblate, Vison Medical), which consisted of four parts: (1) a 2.45 GHz microwave generator with modulated output powers ranging from 5 W to 100 W; (2) a flexible cable; (3) an internal cool-shaft slot antenna (MTC-3CA-II24) which was 14 gauge and 180 mm in length; (4) a peristaltic pump which prevented overheating of the antenna by driving the sterile water running at a constant rate (100 rpm) inside the shaft of the antenna.

Before positioning the antenna, the respiratory-gated axial and sagittal T1-true fast imaging in steady-state precession (truFISP) was routinely acquired to determine the entry point and the antenna trajectory. The T2-half-Fourier acquisition single-shot turbo spin-echo (HASTE) sequence was also performed. The acquisition parameters were chosen as follows: T1 truFISP: time to echo (TE) 3.17 ms, repetition time (TR) 2000 ms, slice 5.5 mm, field of view (FOV) 320 × 256, matrix 256 × 205, flip angle 15°, bandwidth 130Hz/pixel. T2 HASTE: TE 84 ms, TR 1000 ms, slice 4 mm, FOV 320 × 256, matrix 256 × 205, flip angle 170°, and bandwidth 425 Hz/pixel. The oil-filled orientation grid, which was a framework composed of crisscrossed small plastic tubes, appeared as hyperintense columns or cross-sectional dots on T1-truFISP and T2-HASTE images. The target area for ablation was determined by consensus of the two operators, which was supposed to be at least 1.5 cm away from a major vessel (defined as the first or second degree branch of the portal or hepatic veins, which was ≥3 mm in axial diameter,²⁴) and the tip of the antenna should be at least 2 cm from the hepatic surface in order to avoid direct contact between the white zone and the hepatic surface. Thereafter, the entry point on the skin was confirmed by counting the columns of the grid. The antenna was pushed progressively into the pre-determined depth and the path was designed as perpendicular to the surface of the liver as possible, in order to facilitate the determination of the antenna insertion direction during gross pathological evaluation. T1-truFISP images were acquired as appropriate to assess the accuracy of the antenna positioning by verifying the deviation of the entry point, the depth of insertion, the actual angle between the antenna and the liver surface, and possible misplacement into the major vessels. This procedure was repeated until the antenna was accurately positioned. Generally, there were 4-6 ablation targets/pig, according to the size of the liver. For each porcine liver, the ablations were performed from the superficial area to deeper area and from the right hepatic lobe to the left hepatic lobe. It usually took 3-5 passes to place the antenna into the target position.

After measuring the area of liver parenchyma available for ablation, based on our empirical ablation protocols in clinical

Main points

- The increase in the long axis, short axis, and the area of the white zone was more likely to be affected by wattage than energy delivery.
- Among all the morphological metrics, the short axis of the white zone was the most sensitive to changes in wattage.
- Of the microcirculation-related parameters, *f* value in the white zones was not sensitive to changes in MWA protocols and had better intra- and inter-observer agreement than *D** value, which is promising in evaluating the instant changes in ablation zones.
- The instant post-ablation *D* value changed differently in each group and seemed to be affected by changes in wattage.

practice for lesions less than 3 cm and recommendation of the manufacturer, the power and the application duration measured at the generator were assigned as five groups: A, 60 W × 5 min (total energy delivery 18000 J); B, 80 W × 3 min (total energy delivery 14400 J); C, 80 W × 5 min (total energy delivery 24000 J); D, 100 W × 3 min (total energy delivery 18000 J), and E, 100 W × 5 min (total energy delivery 30000 J), in an attempt not to extend the MWA zone from the liver parenchyma to the adjacent large vessels. The ablation was performed with different MWA protocols randomly distributed in the same pig. The total energy delivery was calculated by multiplying power (measured in watts) by duration (measured in seconds). There was an estimated 20% of attenuation of power applied to each target area because of cable losses and antenna reflection.

Acquisition and post-processing of IVIM

After placement of the antenna, the respiratory-triggered IVIM-DW images were obtained before and instantly after MWA, using a single-shot echo-planar imaging pulse sequence. The parallel imaging and spectral presaturation with inversion recovery technique were employed. The diffusion gradients were applied in three orthogonal directions. Seven b values were used, including 50 s/mm², 100 s/mm², 150 s/mm², 200 s/mm², 400 s/mm², and 800 s/mm². Other acquisition parameters included: TE 79 ms, TR 1000 ms, slice 6 mm, FOV 320 × 241, matrix 138 × 138, flip angle 90°, and bandwidth 1726 Hz/pixel. Three continuous slices, with the central slice containing the antenna, were acquired to make the images comparable to gross evaluation. Post-ablation T1-truFISP and T2-HASTE imaging were also performed.

The raw data were transferred to the vendor-supplied MR Body Diffusion Toolbox Veision1.3.0 (Siemens Healthcare) and the parameters, including D , f , and D^* values were automatically mapped pixel-by-pixel according to the biexponential fitting equation as follows²⁵:

$$SI/SI_0 = (1 - f) \cdot \exp(-b \cdot D) + f \cdot \exp(-b \cdot D^*);$$

while the ADC value was calculated using a monoexponential fitting equation as follows:²⁶

$$SI/SI_0 = \exp(-b \cdot ADC),$$

where SI was the signal intensity of IVIM sequence observed at any b value > 0 s/mm², and SI_0 was the signal intensity of IVIM sequence observed at b value = 0 s/mm².

Two radiologists (Reader A with 5 years of experience and Reader B with 10 years) independently measured the IVIM-DWI parameters.

According to a previous report, the post-ablative central coagulative necrotic white zone is hypointense on T2-weighted imaging, and the surrounding red zone appears as a hyperintense rim.²⁷

Two operator-defined regions of interest (ROI_{1,2}) were respectively placed upon the white zones (areas of coagulative necrosis) on bilateral sides of the antenna on post-operative IVIM images (b value = 0 s/mm²), with reference to the T2-HASTE images, avoiding the artifact and large hepatic vessels. Then the ROIs were copied to the same slice of the preoperative IVIM images. The corresponding f , D , D^* , and ADC parameters were automatically measured and the averages calculated from bilateral ROIs were regarded as their final measurements of the white zones.

To determine whether the IVIM parameters can differentiate the white and red zones, another two operator-defined regions of interest (ROI_{3,4}) were respectively placed upon the red zones (areas of surrounding inflammation) on bilateral sides of the antenna on postoperative IVIM images (b value = 0 s/mm²) and the averages calculated from bilateral ROIs were regarded as their final measurements of the red zones (Figure 1).

To compare the test-retest variability of IVIM parameters, an ROI₅ was placed in the adjacent normal parenchyma on post-operative IVIM images (b value = 0 s/mm²) and copied to the same slice of the preoperative IVIM images.

Reader A measured the parameters twice and Reader B measured once for intra- and inter-observer agreement.

Gross evaluation of the MWA zones

The animals were sacrificed immediately after routine post-ablation MRI scan. The MWA zones were labeled with their corresponding MWA protocols and MR images according to their locations in different hepatic segments and body surface markers left by the antennas. The ablation lesions were cut into two halves along the antenna track. A typical MWA zone consisted of

a central white zone (coagulative necrosis) and a peripheral red ring (hyperemic zone, where inflammation and nonlethal hyperthermic injury occurred)²⁸ (Supplemental Figure 1).

The morphological metrics were measured on gross specimen images by two independent readers (Readers A and B, as above) using Image J 1.48V (National Institutes of Health, Maryland, USA), a Java-based application for image processing and analysis (<https://imagej.nih.gov/ij/index.html>) which facilitated measuring the lengths and areas of lesions. A ruler was placed beside the gross specimen for scale calibration when taking the images of gross specimens. The long and short axes of the white zone (WL and WS) were defined as the largest diameter parallel/perpendicular to the track of the antenna, respectively. The area of the white zone (WZ) was calculated by manually outlining it on Image J 1.48V. The sphericity ratio (SR) was defined as WS/WL.¹³ A SR closer to 1.0 is indicative of a more spherical MWA zone.

Statistical analysis

The Bland-Altman test was performed to determine the test-retest variability of the IVIM parameters in normal hepatic parenchyma.

The intra- and inter-observer agreement of morphological metrics and IVIM parameters of the MWA zone were tested with the intraclass correlation coefficient (ICC). The intra- and inter-observer agreement could be classified as poor (ICC < 0.40), fair to good (0.40 ≤ ICC ≤ 0.75), and excellent agreement (ICC > 0.75).²⁹

Morphological metrics among the five groups were compared with Kruskal-Wallis H -test. And Dunn-Bonferroni test was used for post-hoc multiple comparison.

The differences between pre- and post-ablation IVIM parameters in both the white and red zones as well as the differences in post-ablation IVIM parameters between the white and red zones were compared with paired-sample t -test.

Correlations among MWA protocols, morphological metrics, and instant post-ablation IVIM parameters in the white zones were tested with Spearman correlation analysis. The degree of correlation was defined as poor if $R_{\text{Spearman}} < 0.25$, fair if $0.25 \leq R_{\text{Spearman}} < 0.5$, moderate to good if $0.5 \leq R_{\text{Spearman}} < 0.75$, and very good to excellent if $R_{\text{Spearman}} \geq 0.75$, respectively.³⁰

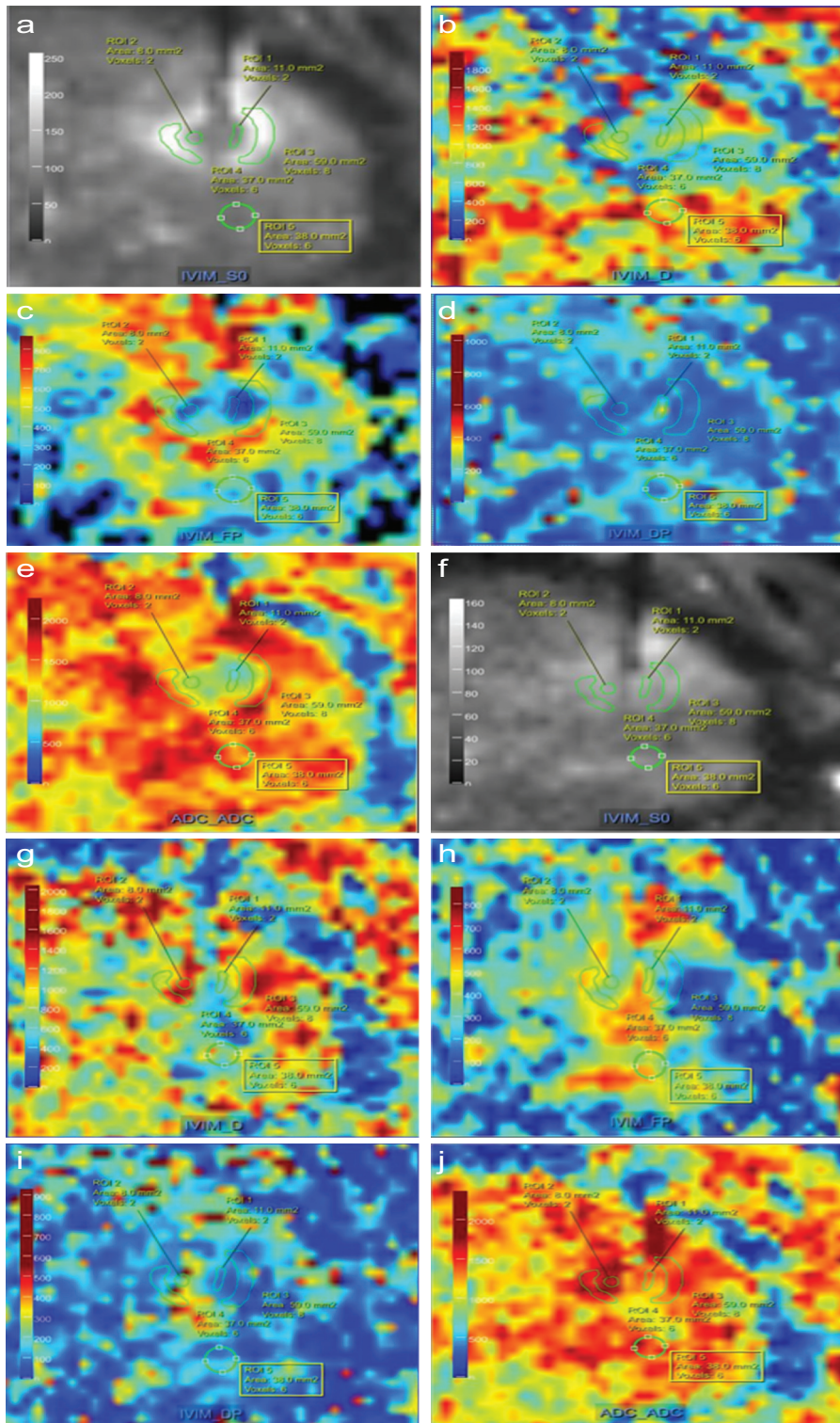


Figure 1. a-j. The ROIs placed on the pre- and post-ablation IVIM-DWI image of a microwave ablation zone produced at 60W × 5min. (a) Post-ablation IVIM image ($b = 0 \text{ s/mm}^2$) showed three sets of ROIs were placed around the track of the antenna (thick black line), including the central coagulative region (ROI1-2) with hypointensity, the peripheral inflammatory reaction region (ROI3-4) with marked hyperintensity, and the surrounding normal liver parenchyma (ROI5). The ROIs were automatically copied to the same slice of corresponding D map (b), f map (c), D^* map (d), and ADC map (e). The ROIs were also copied to the same slice of pre-ablation IVIM image ($b = 800 \text{ s/mm}^2$) (f) and corresponding parametric maps, including D map (g), F map (h), D^* map (i), and ADC map (j). ROI = region of interest.

The statistical analysis was made with SPSS v. 25.0 (IBM Corp.) and Medcalc Software (MedCalc). Statistical significance was considered if $P < .05$.

Results

The average time for each ablation procedure was $52 \pm 21 \text{ min}$, while the average time for antenna placement was $32 \pm 19 \text{ min}$.

The mean width of antenna-induced artifact was $5.05 \pm 1.45 \text{ mm}$ on pre-MWA IVIM images ($b = 0 \text{ s/mm}^2$) and $4.93 \pm 1.58 \text{ mm}$ on post-MWA IVIM images ($b = 0 \text{ s/mm}^2$).

The Bland-Altman test (Figure 2) showed that most of the plots of absolute difference were within the 95% limits of agreement, which suggested that the test-retest variability of the IVIM parameters in normal hepatic parenchyma was acceptable in our study.

The ICCs in measurement of morphological metrics and IVIM parameters of the ablation zones were presented in Table 1. The intra- and inter-observer agreements were excellent in both the morphological metrics and preoperative IVIM parameters.

The morphological metrics of the MWA zones were all expressed as median and interquartile range due to the relatively low number of ablation lesions.

The Kruskal-Wallis test showed significant difference in WL ($P = .014$), short axis (WS) ($P = .001$), and WZ ($P = .003$) of the white zone among the five groups, but the difference in SR was not significant among the five groups ($P = .38$) (Supplemental Figure 2).

The medians, interquartile ranges, and results of the Dunn-Bonferroni post-hoc multiple comparison of the morphological metrics among the five groups were summarized in Table 2. Generally, the WL, WS, and WZ had a tendency to rise from group A to group E. However, Dunn-Bonferroni post-hoc only showed significant differences in WS between group A vs. C, D, and E; in WL between group A vs. E; and in WZ between group A vs. D and E in a multiple comparison.

The paired-samples comparison of IVIM parameters was shown in Table 3.

The microcirculation-related parameters, f and D^* values in the white zones, significantly decreased in all of the five groups after ablation, and they were significantly lower than the f and D^* values in the red zones.

After ablation, D value of the white zone significantly decreased in group A, but significantly increased in Groups C, D, and

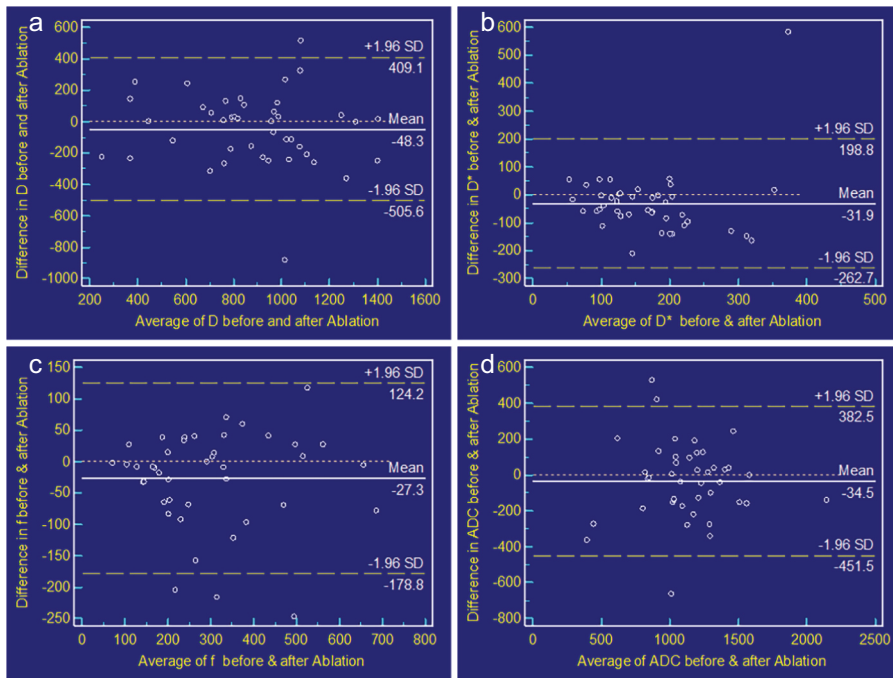


Figure 2. a-d. Test-retest variability of intravoxel incoherent motion parameters measured before and after ablation. Bland–Altman plots showed the test-retest variability of D value (a), f value (b), D* value (c), and ADC value (d) in normal hepatic parenchyma before and after microwave ablation, respectively. The white lines indicated mean absolute difference, while yellow dashed lines indicated 95% limits of agreement.

E. Similar tendency could be observed in ADC value, but significant difference was only noted in group A.

The result of correlation analysis was shown in Table 4.

There was fair positive correlation between energy delivery and WL ($R_{\text{Spearman}} = 0.350, P = .023$) and WS ($R_{\text{Spearman}} = 0.387, P = .011$).

$= 0.350, P = .023$) and WS ($R_{\text{Spearman}} = 0.387, P = .011$).

There was moderate to good positive correlation between wattage and WL ($R_{\text{Spearman}} = 0.504, P = .001$), WS ($R_{\text{Spearman}} = 0.581, P < .001$), and WZ ($R_{\text{Spearman}} = 0.573, P < .001$).

There was moderate-to-good positive correlation between wattage and D value ($R_{\text{Spearman}} = 0.565, P < .001$), ADC value ($R_{\text{Spearman}} = 0.539, P < .001$), but fair correlation among energy delivery, D value ($R_{\text{Spearman}} = 0.315, P = .042$), and ADC value ($R_{\text{Spearman}} = 0.333, P = .031$).

Discussion

Currently, there are no recommended MWA protocols for a larger and more spherical MWA zone, and it remains to be specified how the total energy delivery, the power, and the application duration play a role in the morphology and instant changes in IVIM parameters in the MWA zones in vivo. The results of our study showed that (1) WL and WS had a tendency to rise with the increase in energy delivery and wattage. However, the higher correlation between morphological metrics and wattage implied that these morphological metrics were more likely to be affected by wattage. (2) Among all the morphological metrics, WS was the most sensitive to changes in wattage. (3) Of the microcirculation-related parameters, f value in the white zones was not sensitive to changes in MWA protocols and had better intra- and inter-observer agreement than D* value, which is promising in evaluating the instant changes in white zones. (4) The instant post-ablation D value changed differently in each group and seemed to be affected by

Table 1. Intra- and inter-observer agreement of morphological metrics and IVIM parameters of the MWA white zone

Parameters	Intraobserver agreement				Interobserver agreement			
	ICC	95% CI	f	P	ICC	95% CI	f	P
Morphological metrics								
Long axis ^a	0.98	(0.97, 0.99)	54.93	<.001	0.96	(0.92, 0.98)	45.57	<.001
Short axis ^b	0.98	(0.96, 0.99)	49.79	<.001	0.91	(0.82, 0.96)	20.82	<.001
Area ^c	0.99	(0.98, 0.99)	95.10	<.001	0.97	(0.93, 0.98)	61.94	<.001
Sphericity ratio ^d	0.90	(0.82, 0.95)	10.15	<.001	0.88	(0.77, 0.93)	8.09	<.001
IVIM parameters								
D	0.96	(0.95, 0.97)	27.76	<.001	0.95	(0.93, 0.96)	19.41	<.001
f	0.96	(0.94, 0.97)	22.21	<.001	0.96	(0.95, 0.97)	23.18	<.001
D*	0.87	(0.84, 0.90)	7.77	<.001	0.76	(0.70, 0.82)	4.23	<.001
ADC	0.97	(0.96, 0.98)	30.84	<.001	0.95	(0.93, 0.96)	19.07	<.001

ADC, apparent diffusion coefficient; CI, confidence interval; ICC, intraclass correlation coefficient; IVIM, intravoxel incoherent motion. For ICC, data were means, with 95% CI provided in parentheses. $P < .05$ indicates statistical significance.

Table 2. Multiple comparison of morphological metrics of the MWA white zones between different groups

Morphological metrics	n	Measurement	P value of pairwise comparisons				
			Group A [60 W × 5 min]	Group B [80 W × 3 min]	Group C [80 W × 5 min]	Group D [100 W × 3 min]	Group E [100 W × 5 min]
Long axis ^a (mm)							
Group A [60 W × 5 min]	6	16.53, 3.69		1.00	.42	.078	.028*
Group B [80 W × 3 min]	7	17.98, 2.32			1.00	.64	.271
Group C [80 W × 5 min]	10	19.37, 6.63				1.00	1.000
Group D [100 W × 3 min]	10	20.71, 4.56					1.000
Group E [100 W × 5 min]	9	20.93, 4.02			P value between the five groups = .014*		
Short axis ^b (mm)							
Group A [60 W × 5 min]	6	13.53, 1.50		.87	.019*	.005*	.0001
Group B [80 W × 3 min]	7	16.33, 3.37			1.00	.85	.355
Group C [80 W × 5 min]	10	17.60, 4.22				1.00	1.000
Group D [100 W × 3 min]	10	18.81, 3.93					1.000
Group E [100 W × 5 min]	9	18.52, 2.99			P value between the five groups = .001*		
Area ^c (mm)							
Group A [60 W × 5 min]	6	185.25, 46.35		1.00	.11	.014*	.005*
Group B [80 W × 3 min]	7	237.45, 79.63			1.00	.54	.276
Group C [80 W × 5 min]	10	257.69, 219.84				1.00	1.000
Group D [100 W × 3 min]	10	325.59, 63.67					1.000
Group E [100 W × 5 min]	9	295.51, 130.84			P value between the five groups = .003*		
Sphericity ratio ^d							
Group A [60 W × 5 min]	6	0.76, 0.20					
Group B [80 W × 3 min]	7	0.91, 0.07					
Group C [80 W × 5 min]	10	0.92, 0.12			P value between the five groups = .38		
Group D [100 W × 3 min]	10	0.89, 0.12					
Group E [100 W × 5 min]	9	0.91, 0.08					

Data were presented as median, interquartile range. Morphological metrics were compared with Kruskal-Wallis *H*-test and Dunn-Bonferroni post-hoc test due to the relatively low number of ablation lesions. *P* value < .05 (marked as *) indicates statistical significance. Group A = 60 W × 5 min (total energy delivery 18000 J); B = 80 W × 3 min (total energy delivery 14400 J); C = 80 W × 5 min (total energy delivery 24000 J); D = 100 W × 3 min (total energy delivery 18000 J), and E = 100 W × 5 min (total energy delivery 30000 J) according to the power and application duration. a-d = parameters of the white zones; n, number of white zones.

changes in wattage. Considering the clinical demand of generating a larger and more spherical white zone within a short period of time,³¹ the present study suggests that the combination of high wattage-short application duration would be a better choice, rather than setting a higher energy delivery with lower wattage-longer application. In addition, our results show that post-ablation IVIM was feasible to evaluate the instant changes in MWA zones.

A major finding of this study was that, although wattage and energy delivery were both correlated with the WL and WS,

wattage seemed to play a more important role in the morphology of the MWA zone. It was speculated that the wattage determined the radius of the heat field of MWA.³² However, the present study also showed that wattage mainly affected the WS, in spite of its correlation with WL and WZ. This may be attributed to the internally water-cooled system that minimized overheating along the shaft and made the most of the energy along the short axis perpendicular to the antenna.^{10,11}

Although it is intuitive that longer application duration may result in larger MWA zones, there was no significant difference between

the 3-minute and the 5-minute duration when the wattage was constant in our study. It seemed contrary to findings of another ex vivo study,¹³ which used the expression $a \cdot \ln(t) + b$ to describe the relationship between application duration and coagulation volume or WS. According to previous studies,^{10,11,33} rapid coagulation and loss of water may reduce further energy deposition by changing the tissue conductivity. The size of the MWA zone thus reached a plateau over time, especially after a balance between heat-sink effect and energy transmission. Therefore, a potential explanation of our findings is that the application duration

Table 3. Comparison of intravoxel incoherent motion diffusion-weighted imaging parameters of the MWA zones between different groups

IVIM parameters	n	White zone			Red zone		P for paired t-test	P for comparing post-MWA white & red zones
		Pre-MWA	Post-MWA	P for paired t-test	Pre-MWA	Post-MWA		
D ($\times 10^{-3}$ mm²/s)								
Group A [60 W \times 5 min]	6	1.17 \pm 0.33	0.90 \pm 0.19	.010*	0.99 \pm 0.11	1.02 \pm 0.19	.77	.087
Group B [80 W \times 3 min]	7	1.06 \pm 0.28	1.07 \pm 0.32	.94	1.06 \pm 0.20	1.11 \pm 0.23	.73	.69
Group C [80 W \times 5 min]	10	0.92 \pm 0.41	1.37 \pm 0.32	.002*	1.11 \pm 0.39	1.37 \pm 0.45	.15	.95
Group D [100 W \times 3 min]	10	0.72 \pm 0.48	1.77 \pm 0.63	.005*	0.86 \pm 0.38	1.65 \pm 0.53	.005*	.61
Group E [100 W \times 5 min]	9	1.12 \pm 0.38	1.55 \pm 0.31	.010*	1.00 \pm 0.39	1.33 \pm 0.35	.041*	.030*
f (%)								
Group A [60 W \times 5 min]	6	23.78 \pm 9.41	7.67 \pm 10.86	.011*	28.38 \pm 15.69	15.56 \pm 8.88	.008*	.010*
Group B [80 W \times 3 min]	7	20.36 \pm 7.91	1.96 \pm 2.87	.003*	22.27 \pm 6.88	21.22 \pm 11.78	.79	.008*
Group C [80 W \times 5 min]	10	35.99 \pm 16.52	5.02 \pm 7.28	<.001*	37.02 \pm 11.45	31.92 \pm 14.52	.34	<.001*
Group D [100 W \times 3 min]	10	50.17 \pm 21.60	3.89 \pm 4.79	<.001*	47.73 \pm 18.77	39.06 \pm 17.22	.091	<.001*
Group E [100 W \times 5 min]	9	40.70 \pm 26.15	13.17 \pm 21.22	<.001*	46.36 \pm 21.92	35.28 \pm 23.84	.012*	<.001*
D* ($\times 10^{-3}$ mm²/s)								
Group A [60 W \times 5 min]	6	159.79 \pm 72.51	55.03 \pm 50.28	.007*	189.41 \pm 85.38	149.52 \pm 41.66	.20	.025*
Group B [80 W \times 3 min]	7	198.08 \pm 93.32	47.47 \pm 33.60	.007*	215.05 \pm 73.13	181.36 \pm 81.06	.030*	.008*
Group C [80 W \times 5 min]	10	129.91 \pm 54.82	44.34 \pm 40.15	<.001*	206.05 \pm 56.31	171.49 \pm 35.79	.11	<.001*
Group D [100 W \times 3 min]	10	222.69 \pm 124.70	34.13 \pm 46.77	<.001*	224.65 \pm 79.43	274.08 \pm 101.17	.24	<.001*
Group E [100 W \times 5 min]	9	229.79 \pm 140.15	58.00 \pm 64.94	.004*	242.79 \pm 95.69	179.13 \pm 53.42	.097	.001*
ADC ($\times 10^{-3}$ mm²/s)								
Group A [60 W \times 5 min]	6	1.34 \pm 0.27	0.97 \pm 0.26	0.003*	1.28 \pm 0.19	1.16 \pm 0.27	.28	.089
Group B [80 W \times 3 min]	7	1.21 \pm 0.25	1.11 \pm 0.35	0.40	1.25 \pm 0.22	1.30 \pm 0.30	.70	.11
Group C [80 W \times 5 min]	10	1.31 \pm 0.44	1.42 \pm 0.33	0.39	1.49 \pm 0.43	1.65 \pm 0.42	.25	.11
Group D [100 W \times 3 min]	10	13.0 \pm 0.49	1.80 \pm 0.62	0.092	1.32 \pm 0.61	2.03 \pm 0.38	.014*	.25
Group E [100 W \times 5 min]	9	1.50 \pm 0.45	1.70 \pm 0.51	0.11	1.48 \pm 0.46	1.76 \pm 0.51	.17	.57

Data are presented as means \pm standard deviations and compared with paired-samples t-test. P value < .05 (marked as *) indicates statistical significance. Group A = 60 W \times 5 min (total energy delivery 18000 J); B = 80 W \times 3 min (total energy delivery 14400 J); C = 80 W \times 5 min (total energy delivery 24000 J); D = 100 W \times 3 min (total energy delivery 18000 J); and E = 100 W \times 5 min (total energy delivery 30000J) according to the power and application duration. ADC, apparent diffusion coefficient; IVIM, intravoxel incoherent motion; MWA, microwave ablation; n, number of ablation zones.

chosen in the present study both fell on the plateau of the duration-size curve, which may have a potential influence upon the conclusions and findings of our study. However, given the fact that longer application durations are used in most protocols,^{5,10-13,31,33,34} our result still has its referential significance in clinical practice.

In IVIM-DWI analysis, the ADC parameter characterizes a combination of different compartments of water molecular diffusion within the tissue. The D value describes the pure Brownian motion of water molecules, which is confined by biological structures such as cell membranous surfaces, fibrotic structures, and macromolecules³⁵ while the f and D* values are more related with the

microcirculation within the tissue. Therefore, it was initially expected that the ADC, D, f, and D* values might decrease in the white zone due to water diffusion restriction and perfusion loss in the coagulative necrotic material, while in the red zone, ADC and D might decrease because of cellular edema, and f and D* might increase because of inflammatory hyperemia.²⁰

However, in our study, the instant post-ablation changes in D and ADC values showed various tendencies according to different wattages applied—increased D and ADC could be noted in several groups. As the quantitative parameters of Brownian movement of water molecules, the correlation among D, ADC values, and temperature

has been observed by previous studies and used for thermometry.²¹⁻²³ It was speculated that a higher wattage might lead to a higher residual temperature around the antenna instantly after MWA, which was associated with increased Brownian movement of water molecules and thus the tendency of higher D value. This implies that D and ADC within the MWA zones may fluctuate with the residual temperature of ablation and therefore cannot be used to describe the instant changes in necrotic area and inflammatory area accurately.

On the other hand, the instant post-ablation microcirculation-related parameters, f and D* values, seemed to be more stable among different MWA protocols. The f and

Table 4. Correlation between MWA protocols, post-ablation IVIM parameters and morphological metrics of the white zone

	Energy delivery		Wattage		Duration	
	R_{Spearman}	P	R_{Spearman}	P	R_{Spearman}	P
Morphology						
Long axis	0.350 ^a	.023*	0.504 ^b	.001*	-0.006	.97
Short axis	0.387 ^a	.011*	0.581 ^b	<.001*	-0.042	.79
Area	0.305	.050	0.573 ^b	<.001*	-0.110	.49
Sphericity ratio	0.118	.46	0.202	.20	-0.050	.75
Post-ablation IVIM parameters						
D	0.315 ^a	.042*	0.565 ^b	<.001*	-0.090	.57
f	0.185	.24	-0.001	.99	0.203	.20
D*	0.035	.83	-0.134	.40	0.135	.40
ADC	0.333 ^a	.031*	0.539 ^b	<.001*	-0.048	.76

Correlation between microwave ablation settings, post-ablation IVIM parameters, and morphological metrics of the white zones was analyzed with Spearman correlation analysis. A P value < .05 (marked as *) indicates statistical significance. IVIM, intravoxel incoherent motion.

^aFair correlation with $0.25 \leq R_{\text{Spearman}} < 0.5$.

^bModerate-to-good correlation with $0.5 \leq R_{\text{Spearman}} < 0.75$.

D* values in the white zones were significantly lower than those in the red zones and the pre-ablation hepatic parenchyma, which could be explained by the interruption of the blood flow in the necrotic area. Since the capillary network was destroyed in the central scar, the lack of perfusion could result in f value decreasing to a “base level”. Therefore, the microcirculation-related parameters were independent to energy deposition in the necrotic area without any significant correlation. The difference in f value between the necrotic white zone and inflammatory red zone was also observed by previous studies,^{16,18} which demonstrated its feasibility as a biomarker in monitoring the therapeutic effect of MWA.

Although it was noted that f value was prone to artifact and image noise, which might be associated with factors such as gas production with the white zone and respiratory movement, our study indicated that f value is most promising in accurately predicting diameter of real MWA white zone. Further investigations are required to determine the cutoff values of white and red zones in different parameter maps.

In spite of the significant changes in D* value, its intra- and inter-observer agreement were the lowest in measurement, which suggested its unreliability in clinical practice since an unrealistic high signal-to-noise ratio is required during the DWI study.³⁶ The lowest reproducibility of D* was also noted in previous studies.^{18,36,37}

There were several limitations in the present study. First, the sample size was relatively small. A larger sample size is required to further confirm our findings. Second, although the intra- and interobserver agreement was acceptable in our study, the standard deviation of IVIM parameters within each group was relatively high, probably due to a small sample size, individual difference, and motion artifacts. Potentially additional information could be more accurately provided by contrast-enhanced T1-weighted imaging, and further studies are required to compare the two techniques. Third, the ex vivo study or comparison with radiofrequency ablation was not performed because this study aimed at identifying the MWA protocol settings associated with the morphological features and instant post-ablation IVIM parameters in MWA. Fourth, this study was performed in normal porcine livers rather than hepatic tumors. However, it provided some prospective references about the influence of MWA protocols for further clinical studies.

In conclusion, the present study showed that WL, WS, and WZ had a tendency to rise with the increase in energy delivery and wattage, but the higher correlation between morphological metrics and wattage implied that these morphological metrics were more likely to be affected by wattage, especially WS. High wattage-short duration, rather than a higher energy delivery with lower wattage, may be a recommended MWA protocol for a larger white zone. Of the

microcirculation-related parameters, the f value in instant post-ablation IVIM-DWI was less affected by different MWA protocols and had better intra- and inter-observer agreement than D* value, which is promising in evaluation of the therapeutic effect of MWA as a stable biomarker.

Financial disclosure

This work was supported by the National Natural Science Foundation for Young Scientists of China [Grant no. 81 701 662], National Natural Science Foundation of China [Grant no. U1301258], Medical Project of Hebei Province [Grant no. 20210445], Science and technology project of Baoding [Grant no. 1951ZF106], and Guangdong Provincial People's Hospital Project 2017 [Grant no.2017bq05].

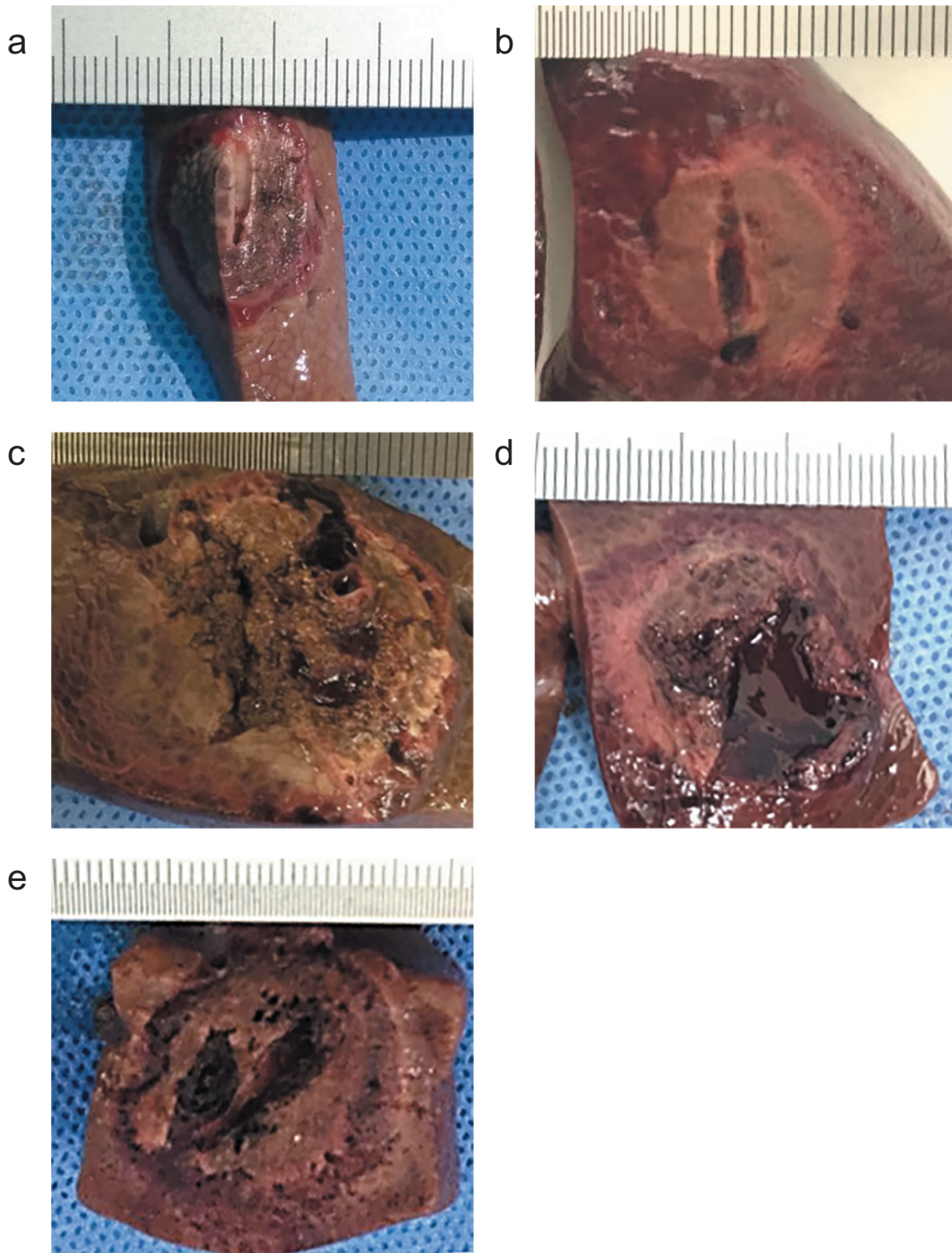
Conflict of Interest disclosure

The authors declared no conflicts of interest.

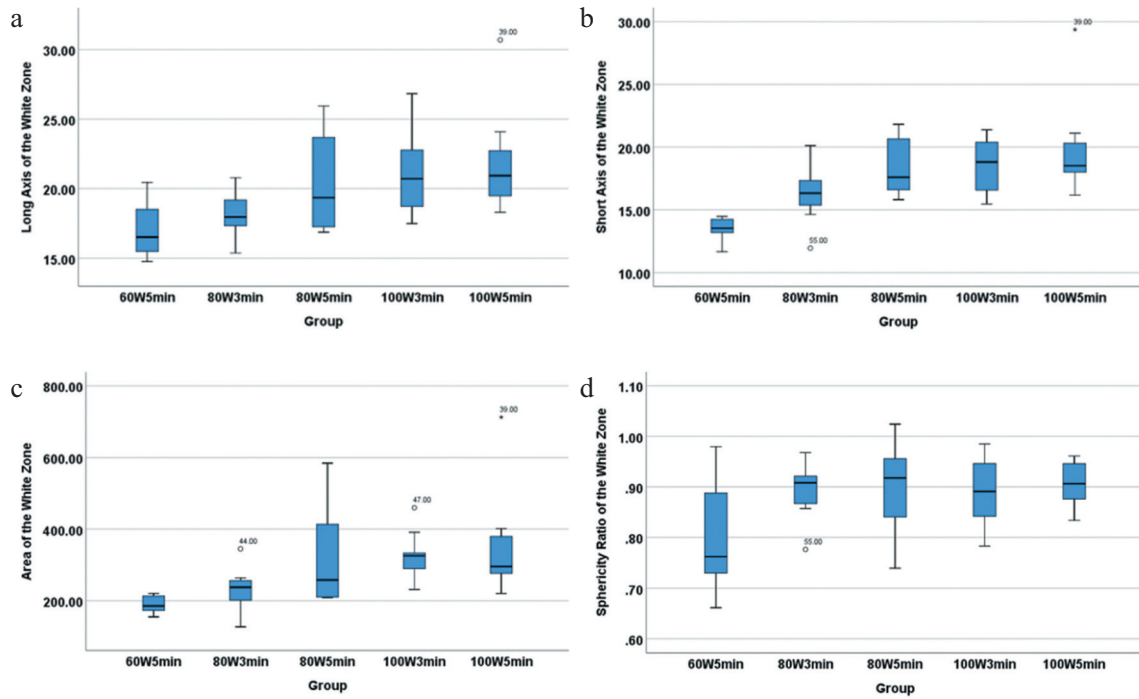
References

- Liang P, Yu J, Lu MD, et al. Practice guidelines for ultrasound-guided percutaneous microwave ablation for hepatic malignancy. *World J Gastroenterol.* 2013;19(33):5430-5438. [Crossref]
- Hoffmann R, Rempp H, Kessler D-E, et al. MR-guided microwave ablation in hepatic tumours: Initial results in clinical routine. *Eur Radiol.* 2017;27(4):1467-1476. [Crossref]
- Chu KF, Dupuy DE. Thermal ablation of tumours: Biological mechanisms and advances in therapy. *Nat Rev Cancer.* 2014;14(3):199-208. [Crossref]
- Correa-Gallego C, Fong Y, Gonen M, et al. A retrospective comparison of microwave ablation vs. radiofrequency ablation for colorectal cancer hepatic metastases. *Ann Surg Oncol.* 2014;21(13):4278-4283. [Crossref]

5. Yu J, Liang P, Yu X, Liu F, Chen L, Wang Y. A comparison of microwave ablation and bipolar radiofrequency ablation both with an internally cooled probe: Results in ex vivo and in vivo porcine livers. *Eur J Radiol.* 2011;79(1):124-130. [\[Crossref\]](#)
6. Shi J, Sun Q, Wang Y, et al. Comparison of microwave ablation and surgical resection for treatment of hepatocellular carcinomas conforming to Milan criteria. *J Gastroenterol Hepatol.* 2014;29(7):1500-1507. [\[Crossref\]](#)
7. He N, Wang W, Ji Z, Li C, Huang B. Microwave ablation: An experimental comparative study on internally cooled antenna versus non-internally cooled antenna in liver models. *Acad Radiol.* 2010;17(7):894-899. [\[Crossref\]](#)
8. Liao M, Zhong X, Zhang J, et al. Radiofrequency ablation using a 10-mm target margin for small hepatocellular carcinoma in patients with liver cirrhosis: A prospective randomized trial. *J Surg Oncol.* 2017;115(8):971-979. [\[Crossref\]](#)
9. Brace CL, Laeseke PF, Sampson LA, Frey TM, van der Weide DW, Lee FT Jr. Microwave ablation with a single small-gauge triaxial antenna: In vivo porcine liver model. *Radiology.* 2007;242(2):435-440. [\[Crossref\]](#)
10. Wang Y, Sun Y, Feng L, Gao Y, Ni X, Liang P. Internally cooled antenna for microwave ablation: Results in ex vivo and in vivo porcine livers. *Eur J Radiol.* 2008;67(2):357-361. [\[Crossref\]](#)
11. Cheng Z, Xiao Q, Wang Y, Sun Y, Lu T, Liang P. 915 MHz microwave ablation with implanted internal cooled-shaft antenna: Initial experimental study in vivo porcine livers. *Eur J Radiol.* 2011;79(1):131-135. [\[Crossref\]](#)
12. Sun Y, Cheng Z, Dong L, Zhang G, Wang Y, Liang P. Comparison of temperature curve and ablation zone between 915- and 2450-MHz cooled-shaft microwave antenna: Results in ex vivo porcine livers. *Eur J Radiol.* 2012;81(3):553-557. [\[Crossref\]](#)
13. Hoffmann R, Rempp H, Erhard L, et al. Comparison of four microwave ablation devices: An experimental study in ex vivo bovine liver. *Radiology.* 2013;268(1):89-97. [\[Crossref\]](#)
14. Dodd GD3rd, Dodd NA, Lanctot AC, Glueck DA. Effect of variation of portal venous blood flow on radiofrequency and microwave ablations in a blood-perfused bovine liver model. *Radiology.* 2013;267(1):129-136. [\[Crossref\]](#)
15. Joo I, Lee JM, Grimm R, Han JK, Choi BI. Monitoring vascular disrupting therapy in a rabbit liver tumor model: Relationship between tumor perfusion parameters at IVIM diffusion-weighted mr imaging and those at dynamic contrast-enhanced MR imaging. *Radiology.* 2016;278(1):104-113. [\[Crossref\]](#)
16. Guo Z, Zhang Q, Li X, Jing Z. Intravoxel incoherent motion diffusion weighted MR imaging for monitoring the instantly therapeutic efficacy of radiofrequency ablation in rabbit VX2 tumors without evident links between conventional perfusion weighted images. *PLoS One.* 2015;10(5):e0127964. [\[Crossref\]](#)
17. Lu TL, Becce F, Bize P, Denys A, Meuli R, Schmidt S. Assessment of liver tumor response by high-field (3 T) MRI after radiofrequency ablation: Short- and mid-term evolution of diffusion parameters within the ablation zone. *Eur J Radiol.* 2012;81(9):e944-50. [\[Crossref\]](#)
18. Shanshan L, Feng S, Kaikai W, Yijun Z, Huiming L, Chuanmiao X. Intravoxel incoherent motion diffusion-weighted MR imaging for early evaluation of the effect of radiofrequency ablation in rabbit liver VX2 tumors. *Acad Radiol.* 2018;25(9):1128-1135. [\[Crossref\]](#)
19. Hoffmann R, Rempp H, Schraml C, et al. Diffusion-weighted imaging during MR-guided radiofrequency ablation of hepatic malignancies: Analysis of immediate pre- and post-ablative diffusion characteristics. *Acta Radiol (Stockholm, Sweden: 1987).* 2015;56(8):908-916. [\[Crossref\]](#)
20. Liu Y, Lu L, Jin H, et al. Radiofrequency ablation of liver VX2 tumor: Experimental results with MR diffusion-weighted imaging at 3.0T. *PLoS One.* 2014;9(8):e104239. [\[Crossref\]](#)
21. Chen J, Daniel BL, Diederich CJ, et al. Monitoring prostate thermal therapy with diffusion-weighted MRI. *Magn Reson Med.* 2008;59(6):1365-1372. [\[Crossref\]](#)
22. Sakai K, Sakamoto R, Okada T, Sugimoto N, Togashi K. DWI based thermometry: The effects of b-values, resolutions, signal-to-noise ratio, and magnet strength. Conference proceedings: Annual International Conference of the IEEE Engineering in Medicine and Biology Society IEEE Engineering in Medicine and Biology Society Annual Conference. 2012;2291-2293.
23. Sakai K, Yamada K, Mori S, Sugimoto N, Nishimura T. Age-dependent brain temperature decline assessed by diffusion-weighted imaging thermometry. *NMR Biomed.* 2011;24(9):1063-1067. [\[Crossref\]](#)
24. Kang TW, Lim HK, Lee MW, Kim Y-S, Choi D, Rhim H. Perivascular versus nonperivascular small HCC treated with percutaneous RF ablation: Retrospective comparison of long-term therapeutic outcomes. *Radiology.* 2014;270(3):888-899. [\[Crossref\]](#)
25. Le Bihan D, Breton E, Lallemand D, Aubin ML, Vignaud J, Laval-Jeantet M. Separation of diffusion and perfusion in intravoxel incoherent motion MR imaging. *Radiology.* 1988;168(2):497-505. [\[Crossref\]](#)
26. Taouli B, Koh DM. Diffusion-weighted MR imaging of the liver. *Radiology.* 2010;254(1):47-66. [\[Crossref\]](#)
27. Lin Z, Chen J, Yan Y, Chen J, Li Y. Microwave ablation of hepatic malignant tumors using 1.5T MRI guidance and monitoring: Feasibility and preliminary clinical experience. *Int J Hypertherm.* 2019;36(1):1216-1222. [\[Crossref\]](#)
28. Song KD, Lee MW, Rhim H, Kang TW, Cha DI, Yang J. Chronological changes of radiofrequency ablation zone in rabbit liver: An in vivo correlation between gross pathology and histopathology. *Br J Radiol.* 2017;90(1071):20160361. [\[Crossref\]](#)
29. Kang KM, Lee JM, Yoon JH, Kiefer B, Han JK, Choi BI. Intravoxel incoherent motion diffusion-weighted MR imaging for characterization of focal pancreatic lesions. *Radiology.* 2014;270(2):444-453. [\[Crossref\]](#)
30. Woo S, Lee JM, Yoon JH, Joo I, Han JK, Choi BI. Intravoxel incoherent motion diffusion-weighted MR imaging of hepatocellular carcinoma: Correlation with enhancement degree and histologic grade. *Radiology.* 2014;270(3):758-767. [\[Crossref\]](#)
31. Imajo K, Tomeno W, Kanezaki M, et al. New microwave ablation system for unresectable liver tumors that forms large, spherical ablation zones. *J Gastroenterol Hepatol.* 2018;33(12):2007-2014. [\[Crossref\]](#)
32. Velez E, Goldberg SN, Kumar G, et al. Hepatic thermal ablation: Effect of device and heating parameters on local tissue reactions and distant tumor growth. *Radiology.* 2016;281(3):782-792. [\[Crossref\]](#)
33. Shi W, Liang P, Zhu Q, et al. Microwave ablation: Results with double 915 MHz antennae in ex vivo bovine livers. *Eur J Radiol.* 2011;79(2):214-217. [\[Crossref\]](#)
34. Dodd GD3rd, Kreidler SM, Lanctot AC, Glueck DH. Effect of change in portal venous blood flow rates on the performance of a 2.45-GHz microwave ablation device. *Radiology.* 2015;277(3):727-732. [\[Crossref\]](#)
35. Lima M, Le Bihan D. Clinical intravoxel incoherent motion and diffusion MR imaging: Past, present, and future. *Radiology.* 2016;278(1):13-32. [\[Crossref\]](#)
36. Lee Y, Lee SS, Kim N, et al. Intravoxel incoherent motion diffusion-weighted MR imaging of the liver: Effect of triggering methods on regional variability and measurement repeatability of quantitative parameters. *Radiology.* 2015;274(2):405-415. [\[Crossref\]](#)
37. Li YT, Cercueil JP, Yuan J, Chen W, Loffroy R, Wang YX. Liver intravoxel incoherent motion (IVIM) magnetic resonance imaging: A comprehensive review of published data on normal values and applications for fibrosis and tumor evaluation. *Quant Imaging Med Surg.* 2017;7(1):59-78. [\[Crossref\]](#)



Supplemental Figure 1. a-e. Pathological specimens acquired from the five groups. Microwave ablation gross specimens acquired from the five groups. (a) 60 W 5 min, white zone 17×13 mm; (b) 80 W 3 min, white zone 17×15 mm; (c) 80 W 5 min, white zone 26×22 mm; (d) 100 W 3 min, white zone 24×20 mm; (e) 100 W 5 min, white zone 19×19 mm.



Supplemental Figure 2. a-d. The tendency of variation in morphological parameters. Box plots demonstrated the tendency of variation in WL (a), WS (b), WZ (c), SR (d) among the five groups. The thick lines were medians of the morphological metrics, and upper and lower hinges represented interquartile ranges. SR, sphericity ratio; WL, the long axis of the white zone; WS, the short axis of the white zone; WZ, the area of the white zone.